Pergamon

International Journal of Multiphase Flow 24 (1998) 693–720

International Journal of Multiphase Flow

The influence of particle rotation on wake stability at particle Reynolds numbers, $Re_P < 300$—implications for turbulence modulation in two-phase flows

J.L. Best

School of Earth Sciences, University of Leeds, Leeds, West Yorkshire, LS2 9JT, UK

Received 2 June 1997; received in revised form 28 October 1997

Abstract

The influence of particle rotation on the stability of the grain wake is investigated experimentally for particle Reynolds numbers less than 300. Particle rotation may be present in most industrial and geophysical two-phase flows and imparts significant differences to the structure of the wake when compared to cases where no rotation is present. An oil-filled flume has been used to investigate the dimensions of the wake region and frequency of wake eddy shedding for isolated, spherical and spheroidal particles at rotation rates up to 10 revolutions/second. A parameter, β, is defined which expresses the ratio of the peripheral surface velocity of the particle to the relative velocity between the two phases. For both shaped particles, the wake is destroyed and absent at $\beta > 0.5$, whilst the size of the wake region is significantly smaller for $0 < \beta < 0.5$ when compared to the wake dimensions at zero rotation. At $0 < \beta < 0.5$ for the spherical grain, the frequency of eddy shedding is modulated and equal to the rotation rate, w, whilst for spheroidal grains this frequency is $2w$ as alternate wakes are shed into the flow as the particle adopts two oblate and prolate orientations in each revolution. At greater rotation rates, an increasingly dominant shear layer is formed on the underside of the grain and generated by fluid being dragged over the rotating particle and sheared against the freestream flow beneath the particle. Where the wake region is destroyed through particle rotation ($\beta > 0.5$), turbulence enhancement in the freestream may still be present due to the generation of this lower shear layer. This work suggests that a principal mechanism of turbulence enhancement by large grains in two-phase flows involves the influence of particle rotation. If particle rotation is present, turbulence enhancement may occur at much lower particle Reynolds numbers than previously assumed, and at higher rotation rates turbulence enhancement of the freestream flow may occur in the *absence* of the wake region. Previous numerical modelling of two-phase flows which invokes wake instability to explain turbulence enhancement in the absence of rotation, may therefore require modification.

Keywords: Particle rotation; Wake instability; Turbulence modulation; Particle asphericity

0301-9322/98/$19.00
PII: S0301-9322(97)00085-2

1. Introduction

Work over the past 15 years has begun to examine and quantify the effects of sediment on the turbulence characteristics of the fluid phase (Rayan 1980; Tsuji and Morikawa 1982; Tsuji et al. 1982, 1984; Hardalupas et al. 1989, 1992; Gore and Crowe 1989a,b, 1991; Hetsroni 1989, 1993; Rashidi et al. 1990; Rogers and Eaton 1990, 1991; Elghobashi and Truesdell 1993; Kulick et al. 1993, 1994; Elghobashi 1994; Yarin and Hetsroni 1994a,b; Kaftori et al. 1995a,b; Crowe et al. 1996; Kenning and Crowe 1997). The influence of sediment on both the mean and turbulent characteristics of the flow, and in particular the attenuation or enhancement of turbulence by the presence of the solid phase, has many important repercussions in both the conveyance of solids in pipes (Bolio and Sinclair 1995), the understanding of earth-surface geophysical flows (Best et al. 1997) and the more complete modelling of two-phase flows (Elghobashi and Truesdell 1993; Elghobashi 1994; Bolio and Sinclair 1995; Kenning and Crowe 1997). Understanding the processes and mechanisms of coupling between the two phases (Crowe 1993) lies at the heart of all of these topics. Several factors have been proposed to explain the modulation of turbulence by the sediment phase including both (i) the size of the particles in relation to the scale of turbulence (Gore and Crowe 1989a,b, 1991; Hetsroni 1989, 1993), and (ii) the particle response time as compared to the turbulence timescale, as expressed through the Stokes number (Elghobashi and Truesdell 1993; Elghobashi 1994; Crowe et al. 1996). In addition, both experimental and theoretical work have demonstrated the significant influence of the sediment mass loading and the grain size distribution on the modulation of turbulence (Yarin and Hetsroni 1994a,b; Kenning and Crowe 1997). Experimental and numerical studies have shown that turbulence enhancement caused by the presence of large sediment grains increases both towards the wall, where particle concentration is greater, and at higher mean sediment loadings (Gore and Crowe 1989a,b, 1991; Yarin and Hetsroni 1994a,b). Several studies have proposed that enhancement of turbulence by sediment larger than the microscale of turbulence is linked to instability of the wake regions associated with the particles, thereby transferring energy from grain movement to the fluid turbulence (Gore and Crowe 1989a,b; Crowe 1993; Hetsroni 1989, 1993; Crowe et al. 1996). This physical mechanism for turbulence enhancement has subsequently been incorporated in several numerical models of turbulence modulation in two-phase flows which have used estimates of both wake length and volume in predictions of turbulence enhancement (Yuan and Michaelides 1992, Bolio and Sinclair 1995). However, in order for this mechanism to be effective, the particle Reynolds number, Re_p, defined using the velocity difference between particle and fluid (Fig. 1), U_{rel}, the grain diameter, D, and the kinematic viscosity of the fluid, ν,

$$\mathrm{Re}_p = \frac{U_{\mathrm{rel}} D}{\nu} \tag{1}$$

must be in the range which is associated with eddy shedding, $\mathrm{Re}_p > 400$ (Achenbach 1974). Whilst wake instability is associated with such high particle Reynolds numbers, these values may be far higher than Re_p values recorded and used in previous studies (Tsuji et al. 1984; Bolio and Sinclair 1995; Best et al. 1997). Hence, although wake instability and eddy shedding may provide a mechanism for fluid turbulence enhancement for $\mathrm{Re}_p > 400$, it is

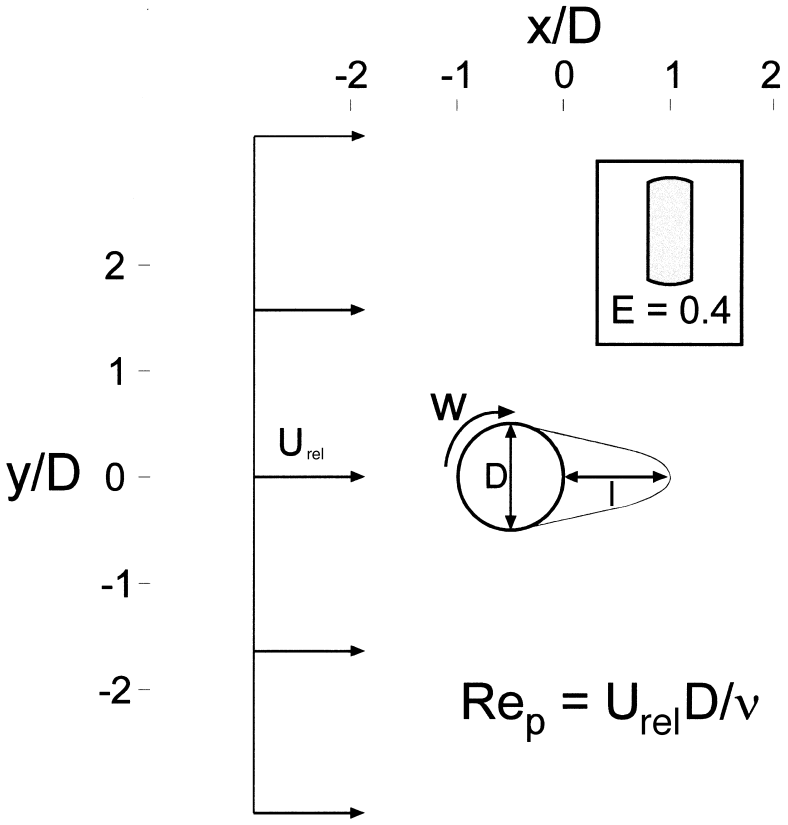

Fig. 1. Definition sketch of rotation of a spherical particle in a shear flow and co-ordinates used in this study. Inset illustrates shape of the spheroidal grain studied here (E = ratio of the short to the long axes of the grain).

likely that this mechanism may not be operative in a wide range of two-phase flows with Re_p below this value. Bolio and Sinclair (1995) suggest that the "wake effect", where turbulence is diffused from a quasi-steady wake, rather than wake shedding, is generating turbulence enhancement, presumably through a grain and its associated wake trailing through the fluid with a relative velocity.

However, in most two-phase flows several factors may serve to make the mechanism of wake instability more complex than that envisaged for simple isolated particles moving with a relative velocity in a shear flow. Firstly, the effect of mutual particle interference in cases where the grain concentration is high, for instance near the wall, may produce complex interactions and modify the stability and shape of the wake region (Tsuji et al. 1982; Zhu et al. 1994; Liang et al. 1996). Kenning and Crowe (1997) have recently stressed the importance of particle interactions and suggested that interparticle spacing may be a key attribute in turbulence modulation. It is likely that both particle–particle and particle-wall interactions may allow enhanced wake instability and this may be reflected by turbulence enhancement that has been documented both in regions of higher grain concentrations near the wall and at higher sediment loadings (Tsuji and Morikawa 1982; Tsuji et al. 1984).

Additionally, all past studies of the wake instability mechanism in two-phase flow have neglected consideration of particle rotation, even though rotation may be expected in all flows where a velocity gradient exists between the top and bottom of the grain and/or where grain interactions and collisions are present. Past studies (Table 1) have documented a range of particle rotation rates, w, in geophysical flows, from 10–40 revolutions second^{-1} (rps) in water flows (Hui and Hu 1991; Lee and Hsu 1994, 1996) to estimates of between 100–1000 rps in air flows (Chepil 1945; White and Schultz 1977; White 1982; Rice et al. 1996) and possibly up to several thousand rps in high-speed compressible flows (White 1986). Particle rotation may be generated by: (i) the shear gradient in the velocity field across the diameter of a grain (Poe and Acrivos 1975), (ii) impacts between grains, whether in suspension or saltation, which may cause rapid rotation commonly in the sense of the shear flow and exceptionally in the opposite direction, and, (iii) impacts between the grains and the solid wall. The latter two cases may generate rotation rates greater than those that can be generated through the shear gradient alone (White and Schulz 1977; Niño and García 1994). Rice et al. (1996) show that particle rotation rates for a coarse sand grain impacting with the bed in an air flow may increase from 330–670 rps before impact to between 430–850 rps after collision.

The influence of particle rotation has been extensively researched in relation to the additional lift force that rotation may impart to saltating grains (White and Schulz 1977;

Table 1
Particle rotation rates documented in previous studies

Author(s)	Fluid	Grain type	Grain size, μm	Rotation rate, w rps	Comments
Francis 1973	Water	Pea-gravel	~4800	~4–5	Estimated from photographs in Francis (plate 20)
White and Schulz, 1977	Air	Glass spheres	350–710	100–300	w measured at a range of flow velocities
White, 1982	Air	Ground walnut shell	600	(i) $w = 387$	(i) normal atmospheric pressure
			600	(ii) $w \sim 400$	(ii) ~50% atmospheric pressure
			1200	(iii) $w = 346$	(iii) ~0.68% atmospheric pressure
Tsuji et al. 1985	Air	Plastic Sphere	5000	34–70	Sphere collision with inclined plate
Lee and Hsu, 1994	Water	Sand	1360	~40	Used w = 40–140 in calculations of saltation height
Lee and Hsu, 1996	Water	Plastic sphere	5950	11–32	w measured at a range of shear velocities
		Glass sphere	4000	17–28	
		Sand	4760	18–27	
		Sand	6540	21–30	
Rice et al. 1996	Air	Sand	425–600	330–670	Before impact with bed
				430–850	After impact with bed

White 1982, 1986; Nalpanis et al. 1993). Grain rotation may lift the grains far higher into the flow than if rotation is absent, this phenomena being known as the Magnus effect (Rubinow and Keller 1961; Saffman 1965; Barkla and Auchterlonie 1971). However, despite the fact that grain rotation may be the norm rather than the exception in most two-phase flows, the influence of grain rotation at low and moderate particle Reynolds numbers has not been considered in relation to turbulence enhancement. Additionally, many studies of turbulence modulation have also used or assumed a spherical grain shape, which is often not the case (see for example Willetts et al. 1982; Willetts 1983, Willetts and Rice 1986) and may impart further complexities into wake instability. For instance, some past experimental work documenting turbulence modulation by the solid phase has used irregular shaped grains (Levy and Lockwood 1981; Tsuji et al. 1984; Shuen et al. 1985) where the influence of grain asphericity may become important.

This paper presents empirical results from an experimental study designed to examine the effect of particle rotation on both spherical and spheroidal particles at $Re_p < 300$. These results demonstrate that particle rotation significantly influences wake instability, and at higher rotation rates the wake is absent. These results suggest that many current numerical models of turbulence modulation and enhancement in two-phase flows may invoke an incorrect physical mechanism for turbulence enhancement, and that terms for the influence of particle rotation and grain asphericity must be incorporated in future simulations.

2. Experimental equipment and methodology

2.1. Experimental set-up

Experiments were conducted in a plexiglas oil-filled recirculating flume (see schematic experimental configuration, Fig. 2) which was 4.50 m long, 0.155 m wide and 0.195 m deep. The pump to the flume was controlled by a voltage controller which allowed precise setting of the oil discharge whilst the flume slope could be adjusted by a screw jack at the top end of the channel. The oil entered the channel and flowed through a baffle plate to minimise any disturbance generated at the flume entrance. A 10 mm diameter test particle was mounted on a 1 mm diameter support wire 2.70 m from the flume entrance and 0.07 m from the base of the flume; this position was chosen where the flow was fully equilibriated and entrance effects were minimal. The ratios of the particle diameter to the flume width and the support wire diameter to the particle diameter were 0.065 and 0.1, respectively, similar to the ranges used in past work (Tsuji et al. 1982). Visual observations and comparison of the wake length (measured as the centreline distance from the downstream edge of the sphere to the furthest downstream point of flow reversal within the wake region) with past work (see below) indicated minimal influence of the support wire on the wake dimensions. The wire mount was fixed in one side wall by a micro-bearing and was tensioned on the outside of the opposite flume wall by a mechanical jig. This support wire was connected to a drive shaft and cog which were driven by either of two stepper motors: these permitted a range of rotation rates, w, from 0.1–100 rps, to be achieved, with the rate being displayed on a digital readout. The accuracy of repeatability in

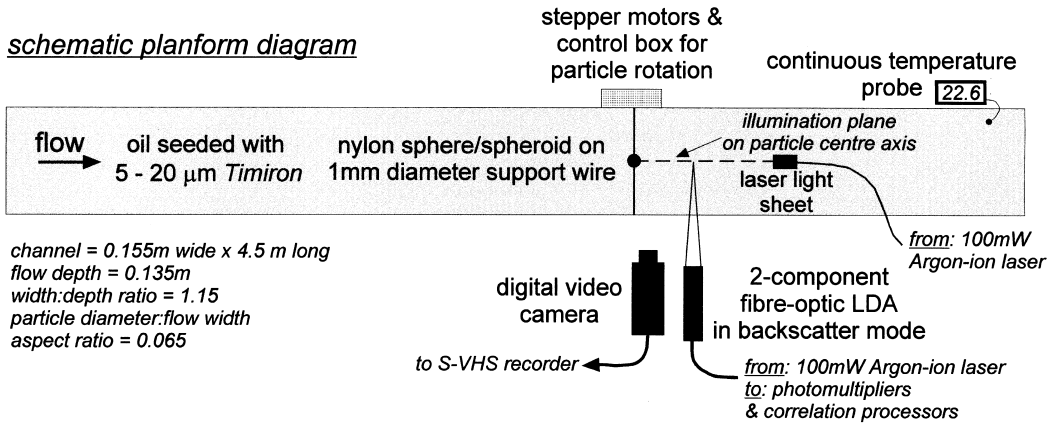

Fig. 2. Schematic planform diagram of experimental equipment.

w was approximately ± 0.1 rps and results from study of rotation rates between 0.5–10 rps are reported herein.

In order to study the influence of particle rotation on wake stability at low and moderate particle Reynolds numbers ($Re_p < 300$) at the velocities possible within the flume, oil was used as the working fluid. The oil used was a clear synthetic base oil, a polyalphaolefin, which was chosen both for its suitable viscosity range (~8 cSt at 20°C) at the room temperatures used in this study, and the fact that its colour and clarity allowed use of laser Doppler anemometry (LDA) and clear video imaging. The temperature dependence of the oil viscosity was determined both from the manufacturers specifications, and from tests using a standard suspended-level type viscometer, with the mean value of kinematic viscosity at each temperature being determined from three measurements. These data were used to construct a viscosity-temperature calibration curve and, with the oil temperature continuously recorded by a thermistor and data logger (Fig. 2) with an accuracy of ± 0.05°C, all viscosity values were determined for the exact temperature of each experiment. The range in oil temperature in these experiments was 20.40–26.45°C.

In this paper results are presented on the influence of particle rotation for two particles of different shape (see Fig. 1 inset) manufactured from Nylon. The first particle had a diameter, $D = 10$ mm, and was spherical in shape with an accuracy in sphericity of ± 0.0127 mm. The second particle studied was manufactured by cutting 3 mm from each of two opposite sides of a 10 mm diameter sphere, thus producing a spheroid with a short axis of 4 mm and a short to long axis ratio of 0.4 (Fig. 1). Each of these nylon particles had a smooth black surface and was mounted on a 1 mm diameter support wire that was drilled through the long axis of the grain. The axis of rotation was at 90° to the mean flow direction, and the sense of rotation the same as in the shear flow, as common in many natural flows (Rice et al. 1996).

2.2. Flow visualisation

In order to allow both determination of wake length and flow patterns around the rotating particles and act as a seed agent for the LDA (see below), Timiron (titanium-coated mica particles) was used as the visualisation agent. The particles were 5–20 μm in diameter and were highly reflective providing excellent flow tracers. A two-dimensional streamwise plane was illuminated using a 100 mW argon-ion laser and fibre-optic light sheet with 40° beam angle lens. This provided an intense light sheet approximately 1 mm thick, and allowed visualisation of flow along the centreline of the sphere. A digital video camera, mounted at the side of the flume, was used to record images which were subsequently downloaded onto S-VHS tape. The digital video camera allowed not only collection of visual data at ordinary video frame rates (25 Hz) but also permitted real time streakline imaging through use of the digital camera exposure time controls. Dependent on the flow velocity, exposure times of between 0.33 and 0.083 s generated excellent real time streakline images of flow in the wake of the particles, which could later be replayed to determine the nature and dimensions of the wake zone. Repeated measurement of wake length dimensions from the video images showed errors of approximately ± 0.05 D. Additionally, long-exposure (0.5–1.0 s) photographs were taken using a 35 mm camera.

2.3. Flow measurement

Velocity and turbulence measurements were taken using a two-component fibre-optic laser Doppler anemometer (LDA) used in back-scatter mode with 161 mm focal length lens and 100 mW argon-ion laser. The LDA was operated with: (1) a 40 MHz frequency shift to enable detection of positive and negative flow directions, and, (2) a DANTEC Particle Dynamics Analyser processor that operates on a correlation-type process. Use of the seed agent yielded data rates between 30 and 1000 Hz, in excess of those desirable to ensure full characterisation of the turbulence spectra (Nezu and Nakagawa 1993). The LDA optics were mounted on a high-precision carriage that could be positioned to within ± 0.025 mm. For the LDA configuration used in this study the resolution of the downstream and vertical components of flow were 0.0027 and 0.0012 ms^{-1}, respectively.

The time series of both the horizontal (downstream), U, and vertical, V, components were used to derive the mean and root-mean-square of each component:

$$\bar{U} = \frac{1}{n} \sum_{i=1}^{n} u_i \tag{2a}$$

$$\bar{V} = \frac{1}{n} \sum_{i=1}^{n} v_i \tag{2b}$$

$$\mathrm{rms}\, u' = \left[\frac{1}{n} \sum_{i=1}^{n} (u_i - \bar{U})^2 \right]^{0.5} \tag{3a}$$

$$\text{rms } v' = \left[\frac{1}{n}\sum_{i=1}^{n}(v_i - \bar{V})^2\right]^{0.5} \tag{3a}$$

where n is the total number of velocity measurements, u_i and v_i are the instantaneous downstream and vertical velocities, $u' = u_i - \bar{U}$ and $v' = v_i - \bar{V}$.

Additionally, the interpolated grids of the mean downstream and vertical components of velocity were used to compute the spanwise vorticity, Ω_z, defined by:

$$\Omega_z = \frac{\partial \bar{V}}{\partial x} - \frac{\partial \bar{U}}{\partial y} \tag{4}$$

2.4. Experimental conditions and procedure

Two series of experiments were conducted, one for the spherical and one for the spheroidal particles (Table 2). The dimensions of the wake region associated with both the spherical and spheroidal particles were determined for a range of particle Reynolds numbers from 29–290 (Table 2), this entailing experiments at a range of mean oil velocities, U_f , (measured 21 particle diameters upstream of the particle) between 0.022 and 0.203 ms^{-1}. For the fixed grains used in this study, the mean flow velocity can be taken as equivalent to the relative velocity between the fluid and sediment phases in mobile bed conditions. The depth of oil in each experiment was kept constant at 0.135 m whilst the flume slope was adjusted so that the bed and oil surface slopes were constant throughout the flume. Several different sets of experiments were conducted for each of the series investigating spherical and spheroidal grains:

2.4.1. Spherical grain.

(*Series 1a*): A series of runs were conducted to visualise the character of the wake at six freestream velocities (0.022, 0.031, 0.041, 0.054, 0.105, 0.149, 0.203 $m\,s^{-1}$) and five particle rotation rates (Table 2) using the digital video camera and laser light sheet. These runs visualised an area downstream of the sphere approximately 10D long and 2 min records for each flow condition were used to determine mean wake length. In all experiments, both without and with particle rotation, the wake length was determined from the position of flow reversal furthest downstream in the leeside of the particle.

(*Series 1b*): In order to construct a detailed quantitative picture of flow in the immediate downstream wake, a grid of 176 LDA points was collected for a freestream velocity, U_f, of 0.105 ms^{-1} ($Re_p \sim 140$) at $w = 0$, 1 and 5 over an area of $y/D = 1.2$ to -3 and $x/D = 1$ to 4 (Fig. 1). No velocities could be collected closer to the sphere than $x/D = 1$ due to interference of the laser beams with both the sphere and the wall-mounted micro bearings. Each point was sampled for 2 min.

(*Series 1c*): At a distance downstream of $x/D = 2$, a series of LDA velocity traverses were taken to examine the changing flow structure in the near-wake area at each freestream velocity and particle rotation rate. Each velocity traverse collected 16 points spaced 2 mm apart from $y/D = 1$ to -2 (see definition diagram, Fig. 1) and each point was sampled for 2 min.

Table 2
Summary of experimental conditions for Series 1 and 2 experiments. Flow depth, Y, was kept constant at 0.135 m in all runs

Series no.	Set	Mean flow velocity, U_f m s^{-1}	Rotation rate, w rps	Mean temperature, T °C	Dynamic viscosity, v St, m s^{-1}	Re	Re$_p$
(1a) Sphere	Wake length	0.022–0.203	0	22.70	0.0752	395–3644	29–270
		0.022–0.203	0.496	21.74	0.0770	386–3559	29–264
		0.022–0.203	1.00	22.23	0.0761	390–3601	29–267
		0.022–0.203	2.02	22.86	0.0749	397–3659	29–271
		0.022–0.203	4.99	25.61	0.0700	424–3915	31–290
(1b) Sphere	LDA grids	0.105	0	23.00	0.0747	1898	141
		0.105	1	23.20	0.0743	1908	143
		0.105	5	22.00	0.0765	1853	137
(1c) Sphere	LDA transects at $x/D = 2$	0.054	0–10	24.10	0.0727	1003	74
		0.105	0–10	23.80	0.0732	1936	143
		0.149	0–10	24.30	0.0723	2782	206
(1 d) Sphere	Time series at $x/D = 2$	0.105	0–10	20.60	0.0792	1790	133
(2a) Spheroid	Wake Length	0.022–0.203	0 (oblate and prolate) - 10	22.80	0.0750	396–3654	29-271 (oblate) 12-108 (prolate)
(2b) Spheroid	LDA transects at $x/D = 2$	0.105	0 (oblate and prolate) - 10	20.60	0.0792	1790	133
(2c) Spheroid	Time series at $x/D = 2$ and $y/D = 0$	0.105	0 (oblate and prolate) - 10	20.25	0.0799	1774	131

(*Series 1d*): In order to examine the detailed time series at a range of rotation rates, at-a-point LDA time series were collected for 10 min in the region of maximum turbulence intensity for a freestream velocity of 0.105 ms^{-1} and at each of the rotation rates of 0, 0.5, 1, 2, 5 and 10 rps.

2.4.2. Spheroidal grain.

(*Series 2a*): The wake character was again examined at six freestream velocities and six particle rotation rates (Table 2). Additionally, the wake character was examined at each freestream flow velocity for $w = 0$ but in an oblate (long axis normal to downstream flow direction) or prolate (long axis parallel to downstream flow direction) orientation. These runs visualised an area downstream of the spheroid approximately $12D$ long.

(*Series 2b*): At $x/D = 2$, a series of velocity traverses were taken at six rotation rates at a mean freestream velocity of 0.105 ms^{-1}. Each traverse sampled 16 points, which were spaced 2 mm apart between $y/D = 1$ and -2, for 2 min. Traverses were also taken for both the oblate and prolate orientations at zero rotation.

(*Series 2c*): At-a-point time series were collected for 10 min at $x/D = 2$ and $y/D = 0$ for a freestream velocity of 0.105 ms^{-1} and at each of the rotation rates of 0 (oblate and prolate orientations), 0.5, 1, 2, 5 and 10 rps.

3. The influence of particle rotation on the wake of spherical grains

3.1. Wake length

Measurements of wake length for $w = 0$ at a range of particle Reynolds numbers (Fig. 3a) shows good agreement with past experimental and numerical estimates (Taneda 1956; Rimon and Cheng 1969; Kalra and Uhlherr 1973; Clift et al. 1978). Slight discrepancies between studies (up to 0.17 l/D, where l is wake length and D is particle diameter, Figs. 1 and 3a) may be attributed to both experimental error in obtaining the mean wake length and the differing experimental conditions between studies. As rotation rate increases at each particle Reynolds number, so the length of the wake region decreases (Figs. 3a and 4). For the particle Reynolds numbers studied here ($Re_p < 300$), no wake was present at rotation rates greater than 5 rps. If wake length during rotation, l_r, is expressed relative to the wake length at the same particle Reynolds number at zero rotation, l_0, and plotted vs. the ratio, β, of the peripheral velocity of the sphere, U_p, to the mean flow (relative) velocity, U_f ($\beta = U_p/U_f$, Fig. 3b), it can be seen that the wake ceases to exist at a peripheral velocity approximately half that of the flow (relative) velocity ($\beta \geq 0.5$; see Fig. 4 also). The relationship between l_r/l_0 and β (Fig. 3) is given by a fitted fourth-order polynomial curve to the data of the form:

$$l_r/l_0 = 1 + -2.28 \cdot \beta + 15.6 \cdot \beta^2 + -56.64 \cdot \beta^3 + 52.48 \cdot \beta^4 \quad (5)$$

Wake generation and eddy shedding may thus be expected to be absent at higher rotation

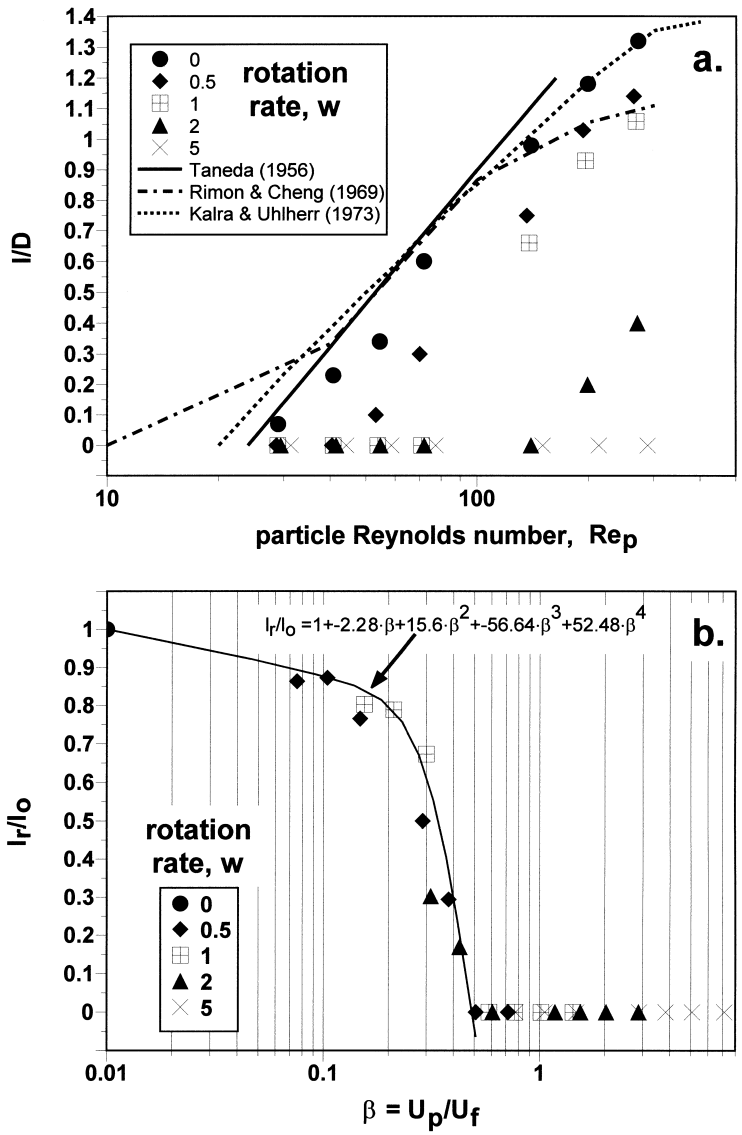

Fig. 3. (a) Relationship between length of the wake separation zone, l/D, and particle Reynolds number, Re_p, for spherical grains at a range of grain rotation rates, w. Data from three past studies are plotted for comparison. (b) Relationship between wake length, l_r/l_0, and the ratio of peripheral velocity of the particle : freesteam flow velocity, β.

rates. Additionally, at lower rotation rates ($0 < \beta < 0.5$) the length, and hence volume, of the wake zone will be greatly different to that estimated at zero rotation and as incorporated in some numerical models of turbulence enhancement (Yuan and Michaelides 1992; Bolio and Sinclair 1995).

3.2. Mean flow field

The nature of the mean flow field was assessed both qualitatively from the video and photographic images (Fig. 4) and quantitatively from three detailed LDA grids for $U_f = 0.105$ ms^{-1} ($Re_p \sim 140$, Table 2) at rotation rates of 0, 1 and 5 rps (Fig. 5) and LDA traverses located at $x/D = 2$ for $w = 0$, 0.5, 1, 2, 5 and 10 (Fig. 6).

Plots derived from the three LDA grids of the mean downstream and vertical velocities, their associated turbulence intensities and vorticity are shown in Fig. 5. All quantities have been made dimensionless through division by the mean horizontal flow velocity, U_f, taken at $x/D = -21$ and $y/D = 0$. At zero rotation, the plots illustrate the characteristic flow field downstream of a bluff body: deceleration downstream from the recirculating wake region (note that at this velocity ($Re_p \sim 140$) the wake length is 0.98 l/D and the laser measurement grid does not extend into this region), flow convergence downstream of the sphere and regions of higher turbulence intensity (especially for the downstream component, Fig. 5a,b) associated with the shear layer on each side of the particle.

Rotation of the particle has a dramatic effect on the flow field; at this mean flow velocity the wake length at $w = 1$ is 0.66D whilst at $w = 2$ and 5 the wake is absent (Figs. 3, 4 and 5). Flow is dragged around the sphere and the mean flow vectors are directed downwards

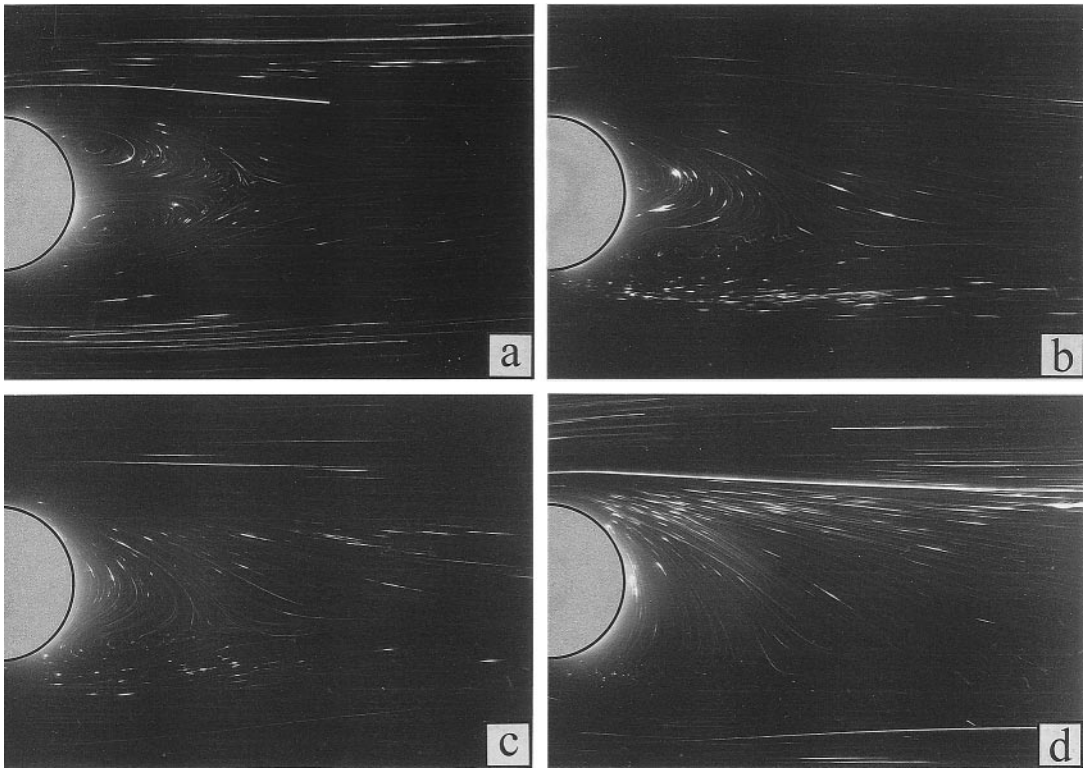

Fig. 4. Visualisation of flow behind a sphere at $Re_p \sim 140$ at four rotation rates. (a) $w = 0$; $\beta = 0$; (b) $w = 0.5$; $\beta = 0.15$; (c) $w = 1$; $\beta = 0.30$; (d) $w = 5$; $\beta = 1.50$.

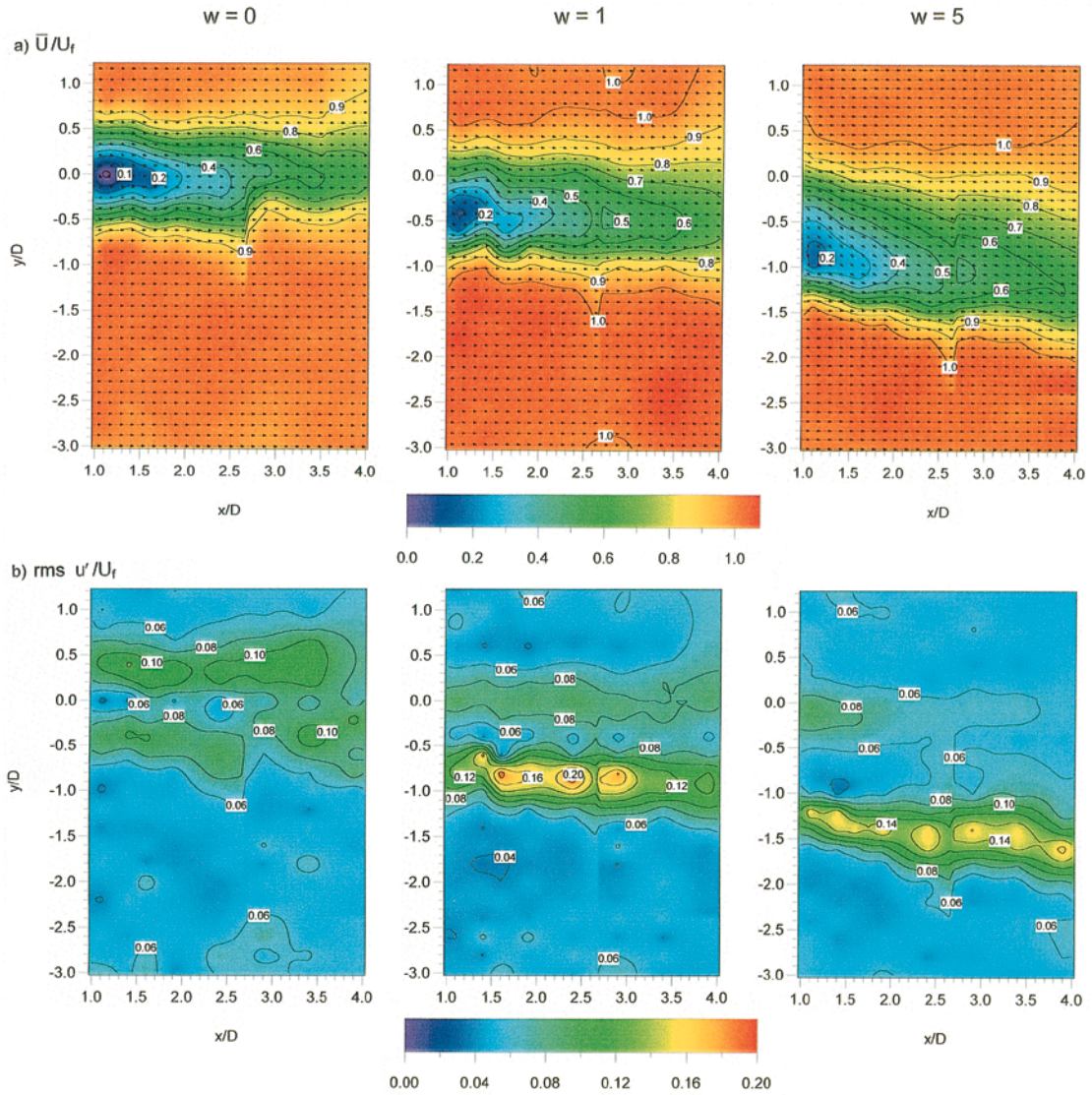

Fig. 5. Maps of mean flow, turbulence intensities and vorticity derived from the LDA grids downstream of the sphere at $U_f = 0.105$ ms^{-1} and $w = 0$, 1 and 5. All quantities have been divided by the mean downstream flow velocity, U_f. (a) Downstream velocity, $\bar{U}/U_f$, and UV vectors; (b) Turbulence intensity of downstream component, rms u'/U_f; (c) Vertical velocity, $\bar{V}/U_f$; (d) Turbulence intensity of vertical component, rms v'/U_f; (e) Spanwise vorticity, Ω_z/U_f.

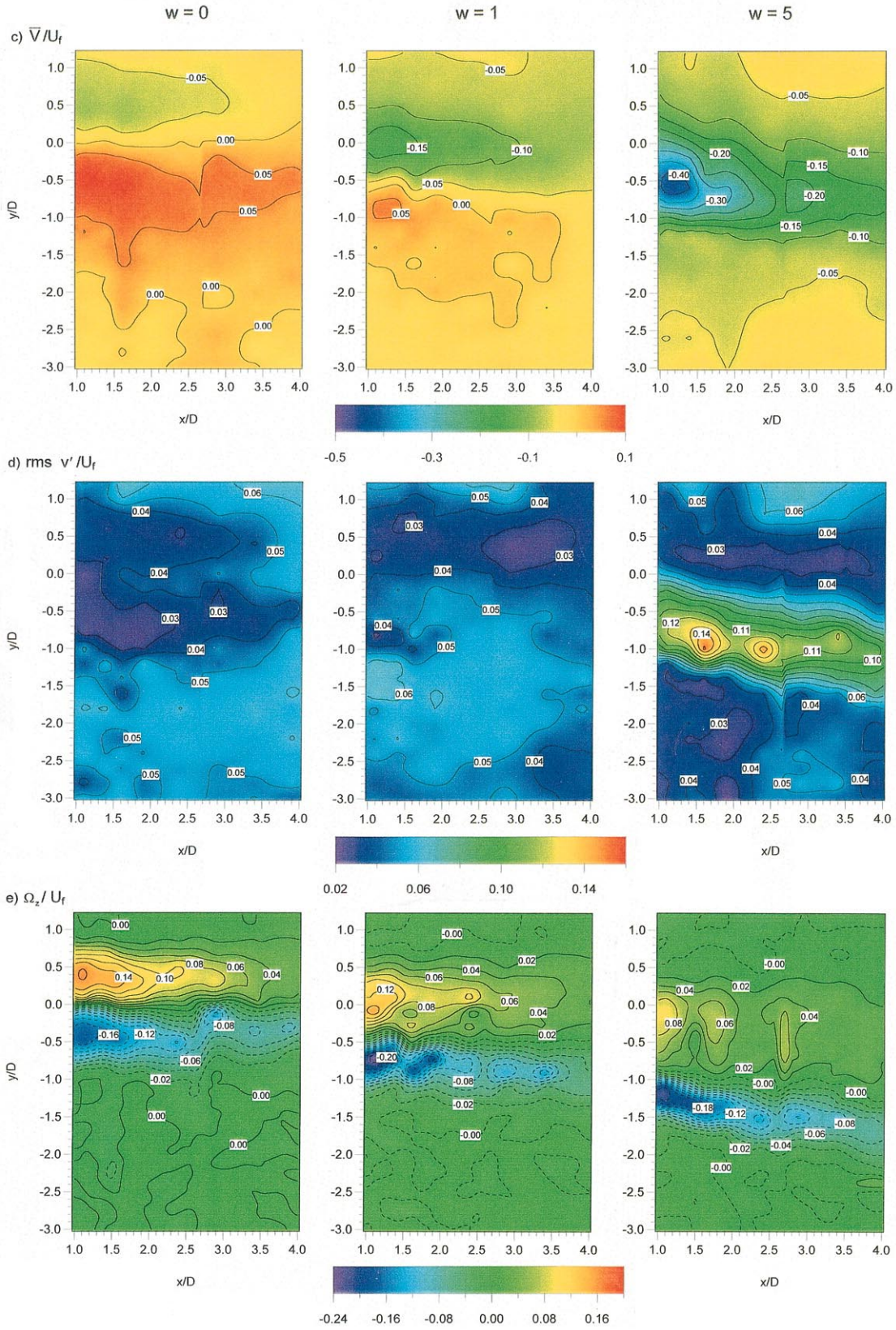

Figure 5 *(caption on page* 705)

downstream of the sphere, especially for $w = 5$ (Fig. 5a). The location of the region of minimum downstream velocity can also be seen to be shifted from $y/D = 0$ at $w = 0$ (a symmetrical wake region) to -0.45 and -0.9 y/D for $w = 1$ and 5, respectively. The turbulence intensity of the downstream velocity component is decreased on the upper side of the particle as rotation rate increases (Fig. 5b) . However, this decrease is accompanied by an increase in the downstream turbulence intensity on the lower side of the grain that is caused by: (i) the lower shear layer of the wake which is still present at $w = 1$ and has become more unstable through rotation, and, (ii) a shear layer formed on the underside of the grain, and located below the lower wake shear layer, where fluid being dragged around the sphere meets flow underneath the particle. This shear layer is generated in the absence of the wake at $w = 5$ and suggests that freestream turbulence enhancement may be generated by rotation *after* the wake region has ceased to exist. The generation of this shear layer due to rotation is most pronounced in the turbulence intensity plots of the vertical component of flow (Fig. 5 d) which, because flow at $w = 5$ is markedly downwards around the sphere (Fig. 5c) where fluid is being entrained by rotation at locations up to $x/D = 4$, generates intense shear where this fluid meets flow on the lower side of the particle. These trends are also evident in the vorticity plots (Fig. 5e) which illustrate the progressive concentration of maximum vorticity on the underside of the particle as rotation rate increases. The zone of maximum vorticity is displaced further below the grain, where the sign of vorticity is also negative due to the direction of the shear gradient on the underside of the grain.

These trends in flow structure around the sphere with increasing rotation rate are revealed by the LDA traverses at $x/D = 2$ for $U_f = 0.05$, 0.10 and 0.15 ms^{-1} ($\mathrm{Re}_p \sim 74$, 143 and 206 respectively) at all rotation rates (Fig. 6). The key points evident from these traverses are:

1. The low velocity region downstream from the sphere is progressively displaced to the underside of the particle as rotation rate increases at all three velocities. For the highest rotation rate measured ($w = 10$) at $U_f = 0.05$ ms^{-1}, the downstream velocity at $y/D = -2.0$ is still $0.48U_f$ but the vertical flow velocity remains markedly negative, illustrating the dominance of the rotation-generated flow at these low particle Reynolds numbers ($\mathrm{Re}_p \sim 74$).
2. At all flow velocities the maximum downstream turbulence intensity becomes located further below the sphere at higher rotation rates. However, it is evident that the highest rotation rates ($w = 10$) are not associated with the highest turbulence intensities but these occur at $w = 1$–5.
3. The peak in turbulence intensity of the vertical component of flow becomes both displaced to the lower side of the grain and attains greater values at higher rotation rates for all mean flow velocities. Additionally, the turbulence intensity of the vertical component increases at higher particle Reynolds numbers (relative velocities) for a given rotation rate.

These results on flow past a rotating sphere match well with past experimental and numerical modelling of flow past cylinders undergoing rotation (Taneda 1978; Townsend 1980; Díaz et al. 1983; Ingham 1983; Badr et al. 1989; Ingham and Tang 1990) which have shown that the flow field behind a circular cylinder is significantly altered by rotation. Some numerical results have indicated that the closed streamlines behind the cylinder are annihilated when the parameter α ($\alpha = (D/2)\omega / U_f$, where D = diameter of sphere or cylinder and ω = angular velocity) exceeds

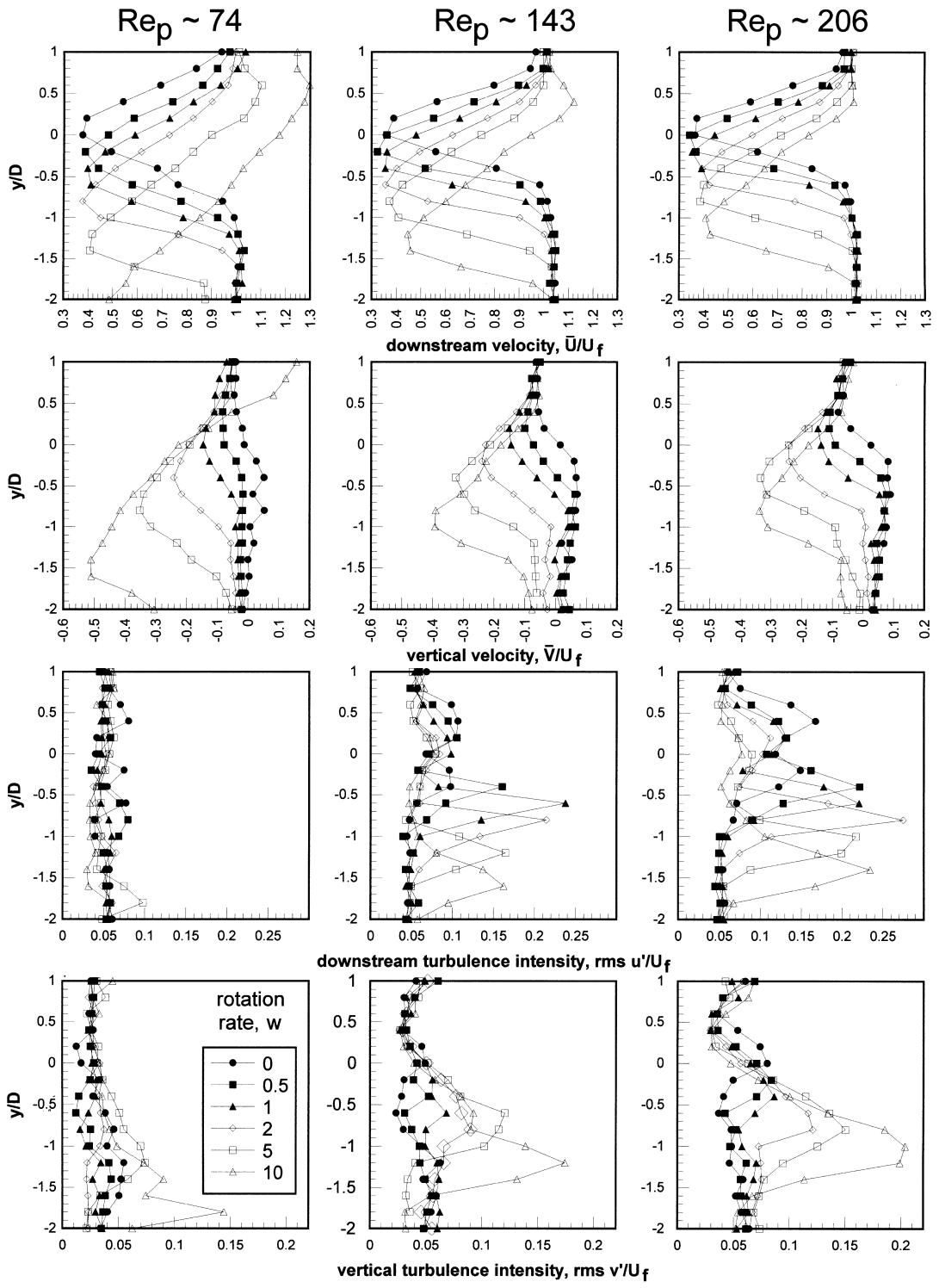

Fig. 6. Profiles of downstream and vertical velocities and their turbulence intensities taken at $x/D = 2$ at three mean flow velocities (U_f=0.054, 0.105 and 0.149 ms^{-1}; Re$_p$~74, 143 and 206 respectively) for $w = 0$, 0.5, 1, 2, 5 and 10.

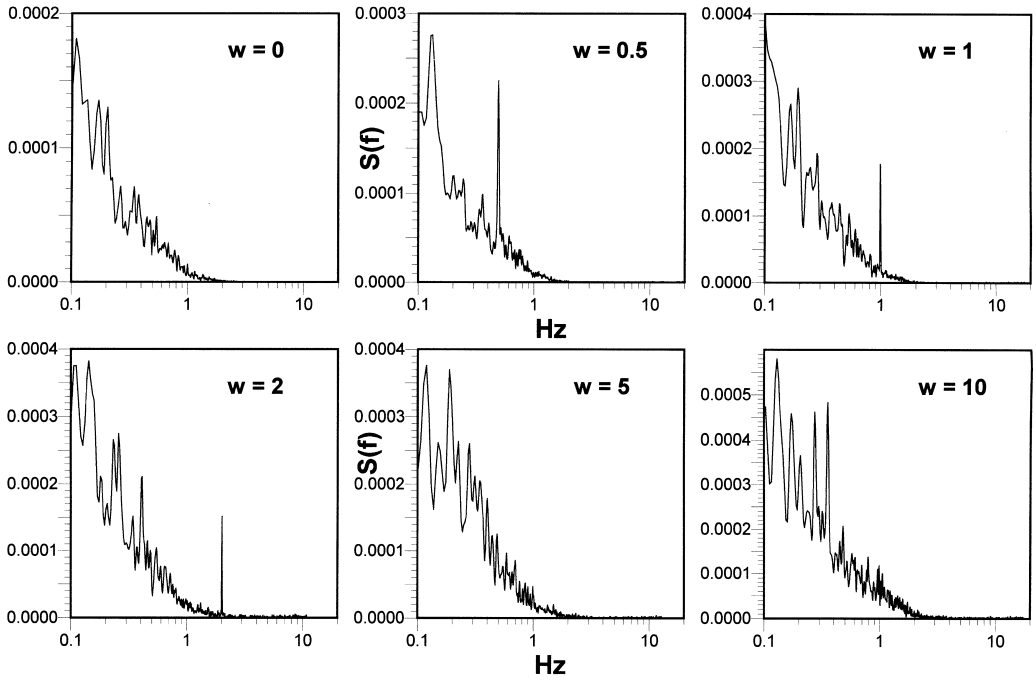

Fig. 7. Frequency spectra (spectral density, $S(f)$) derived from 600 s time series at $U_f = 0.105$, $w = 0$, 0.5, 1, 2, 5 and 10 and $x/D = 2$. Points taken at $y/D = -0.4$, -0.4, -0.6, -0.6, -0.8, -1.2 and -1.6 for $w = 0$, 0.5, 1, 2, 5 and 10 respectively.

0.5 (Ingham 1983; Ingham and Tang 1990) and that as α increases a larger volume of fluid rotates with the cylinder. These results find parallels in the present study, where the entrainment of flow around the sphere increases at higher values of β and the wake region ceases to exist at $\alpha \sim 1$. The experimental work of Díaz et al. (1983) also demonstrated that the cylinder wake ceased to exist at $\beta > 1$ for $\mathrm{Re}_p = 9000$. Although there are clear differences in the flow field behind cylinders and spheres which cause differences in the β values at which the wake disappears, the trends in wake evolution, eddy generation and wake annihilation are largely identical between cylinders and spheres as rotation rate increases.

3.3. At-a-point time series and spectra

Frequency spectra obtained from the downstream component of velocity measured in the region of maximum turbulence intensity for $U_f = 0.105$ ms^{-1} at $w = 0$, 0.5, 1, 2, 5 and 10 are illustrated in Fig. 7. The spectra were derived from 600 s records with a sampling rate of between 40 and 100 Hz and processed using the resampling and interpolation methods detailed in DANTEC (1994). A resampling rate of $1/t_s$, where t_s is the mean sampling interval, was applied to all signals and the spectra were filtered using a Tukey window. The spectra at zero rotation shows no distinct peak but a range of values with most energy being contained in frequencies less than 1 Hz. However, rotation of the sphere produces a clear peak in frequency

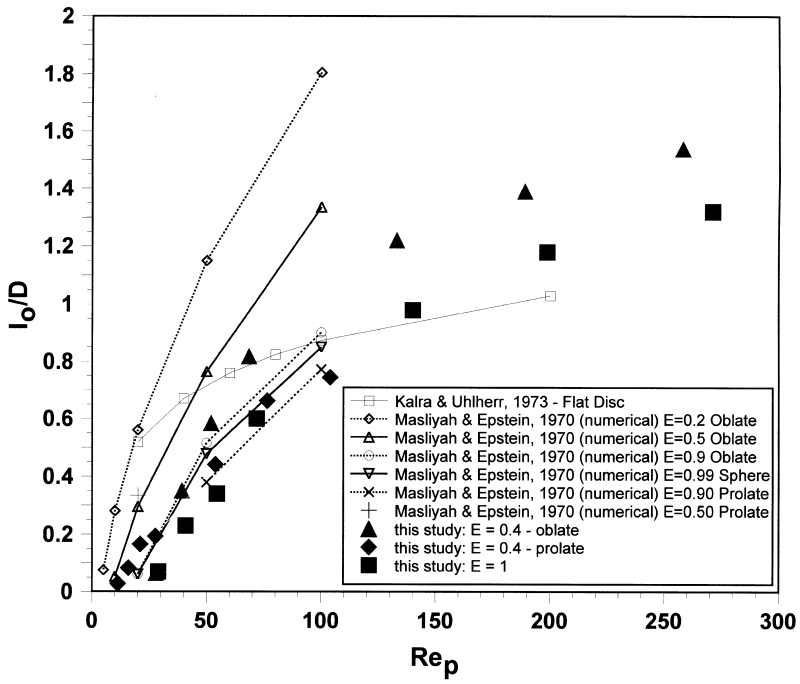

Fig. 8. Relationship between wake length and particle Reynolds number for spheroid at $w = 0$ in both oblate and prolate orientations with respect to the mean flow. Previous determinations of wake length behind spheroids and discs are plotted for comparison.

for $w = 0.5$, 1 and 2 at the frequency of the rotation rate, although the peak is less distinct at $w = 2$. This clear peak is associated with wake instability modulated by the frequency of rotation. However, at $w = 5$ and 10, corresponding to β of 1.5 and 3, respectively, which have been shown previously to be conditions where no wake exists behind the sphere (Figs. 3–5), the clear spectral peak has disappeared and turbulence is dominated by lower frequency components. The absence of spectral peaks at $w = 5$ and 10 illustrates that the clear dominance of the spectra at lower rotation rates is due to wake instability modulated by rotation.

The numerical work of Badr et al. (1989) concerning flow past rotating cylinders has shown that at higher particle Reynolds numbers ($Re_p > 60$), flow behind a rotating cylinder does not tend to a steady state with time from the start of rotation, but rather develops a periodic pattern of vortex shedding. Additionally, the experimental work of Díaz et al. (1983) has shown the strong modulation of eddy shedding through cylinder rotation; at low rotation rates ($\beta < 1$) the cylinder wake flow is dominated by a process of modified eddy shedding whereas at higher rotation rates ($\beta > 1$) the flow does not possess any Kármán vortex street activity. These trends are also borne out in the present study, where strong modulation of eddy shedding downstream of the sphere is present at rotation rates of $\beta < 0.5$, whereas at $\beta > 0.5$ such modulation and separation zone wake instability are absent.

4. The influence of particle rotation on the wake of spheroidal grains

Many, if not most, grains in a wide range of industrial and geophysical boundary layers are non-spherical and may be associated with markedly non-uniform flow patterns during grain rotation. Past studies of turbulence modulation have employed both spherical grains (Tsuji and Morikawa 1982; Tsuji et al. 1984) but also more irregular grains, such as natural sand (Levy

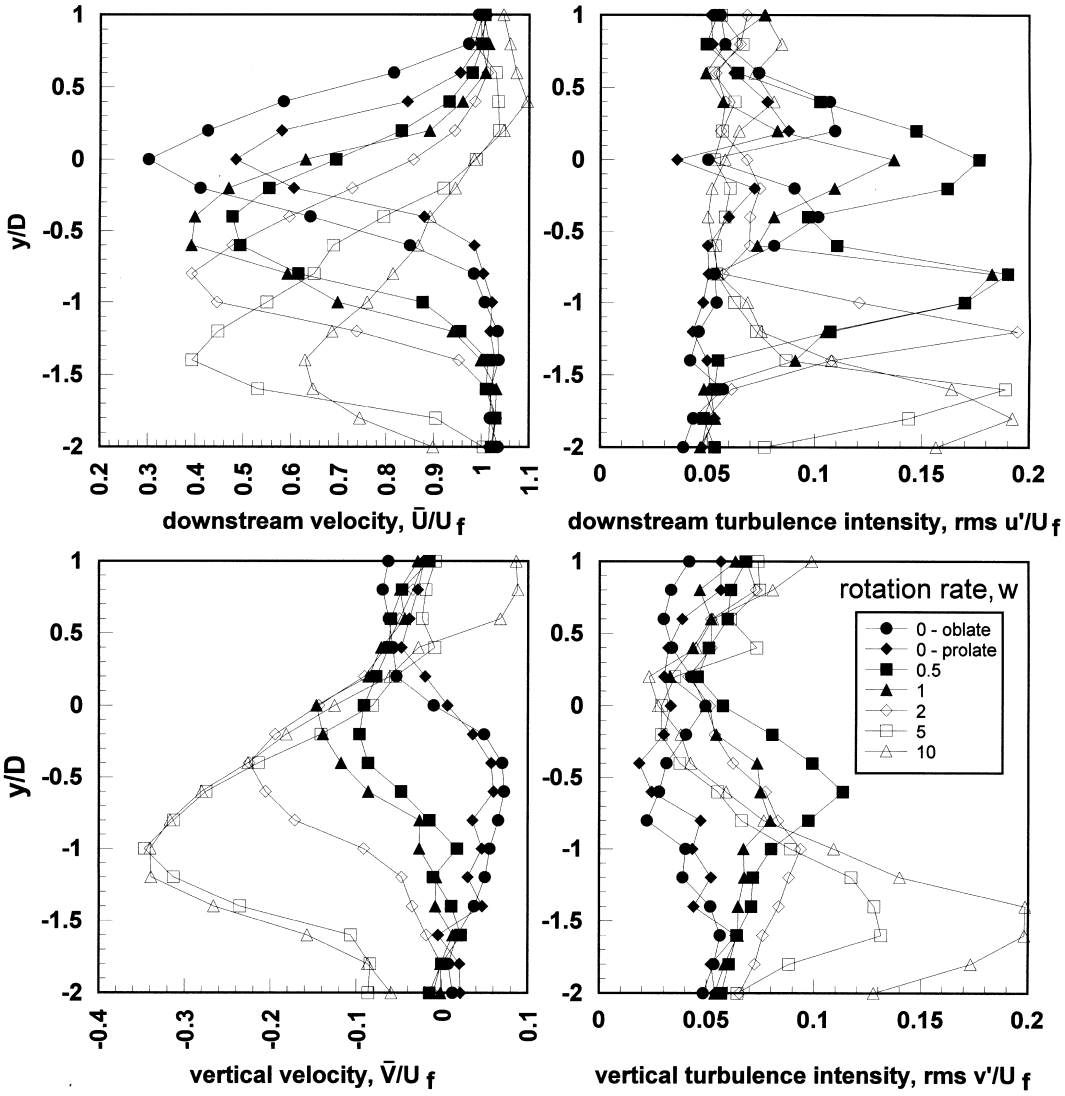

Fig. 9. Profiles of downstream and vertical velocities and their turbulence intensities taken at $x/D = 2$ downstream of a spheroid at $U_f = 0.105$ ms^{-1} for $w = 0$, 0.5, 1, 2, 5 and 10.

and Lockwood 1981) and cylindrical grains (Tsuji et al. 1984). In order to investigate the patterns of flow associated with a non-spherical grain, a brief series of experiments were conducted with a spheroidal grain ($E = 0.4$, Fig. 1) to examine the influence of particle rotation on wake stability and turbulence production.

4.1. Wake length

Wake length behind the spheroid was measured at all flow velocities with the spheroid in both an oblate and prolate orientation and the axis of rotation normal to flow. As expected, wake length increases with particle Reynolds number, with wake length in the oblate position being approximately 2–4 times longer than in the prolate orientation at the same flow velocity (the long and short ($0.4D$) axes of the spheroid are used for the oblate and prolate orientations respectively to calculate l_0/D and Re_p on Fig. 8). These measurements correspond well (Fig. 8) with past numerical and experimental determinations of wake dimensions associated with spheroids in different orientations (Masliyah and Epstein 1970; Masliyah 1972; Clift et al. 1978) and flow around flat discs (Kalra and Uhlherr 1973).

Observations from the digital video recording illustrated a regular process of wake shedding during particle rotation such that it was very difficult to estimate average wake length during rotation. As the particle rotated, a larger wake was created when the particle long axis was in an oblate orientation normal to the flow but this wake was shed into the flow as the particle moved into a prolate position parallel to the flow. Rotation therefore caused regular shedding of the large wake region generated when the spheroid was in an oblate orientation.

4.2. Mean flow field

Velocity transects at $x/D = 2$ for $U_f = 0.105$ ms^{-1} and $w = 0$, 0.5, 1, 2, 5 and 10 are shown in Fig. 9. The symmetrical structure of the wake in both oblate and prolate positions is again clearly evident with both the velocity reduction at $x/D = 2$ and the turbulence intensity in the shear layer on either side of the particle being greater for the oblate than the prolate position. As the spheroid is rotated, similar trends in the velocity profiles are evident as described above for the spherical particle. The low velocity wake region becomes displaced to progressively more negative y/D values and the turbulence intensity of both the downstream and vertical velocity components strongly increases on the underside of the particle at higher rotation rates. The turbulence intensity of the downstream velocity component on the upper side of the particle decreases with rotation rate and at $w = 2$ ($\beta \sim 0.60$) these values are essentially close to the freestream values. The vertical velocities show marked downward flow over the particle at higher rotation rates and high turbulence intensity along the shear layer formed on the underside of the particle.

4.3. At-a-point time series and spectra

Time series collected at $x/D = 2$ and $y/D = 0$ for $U_f = 0.105$ ms^{-1} for all rotation rates reveal the remarkable modulation of vortex shedding into the free flow by particle rotation. Representative segments of the time series (Fig. 10) illustrate that particle rotation modulates

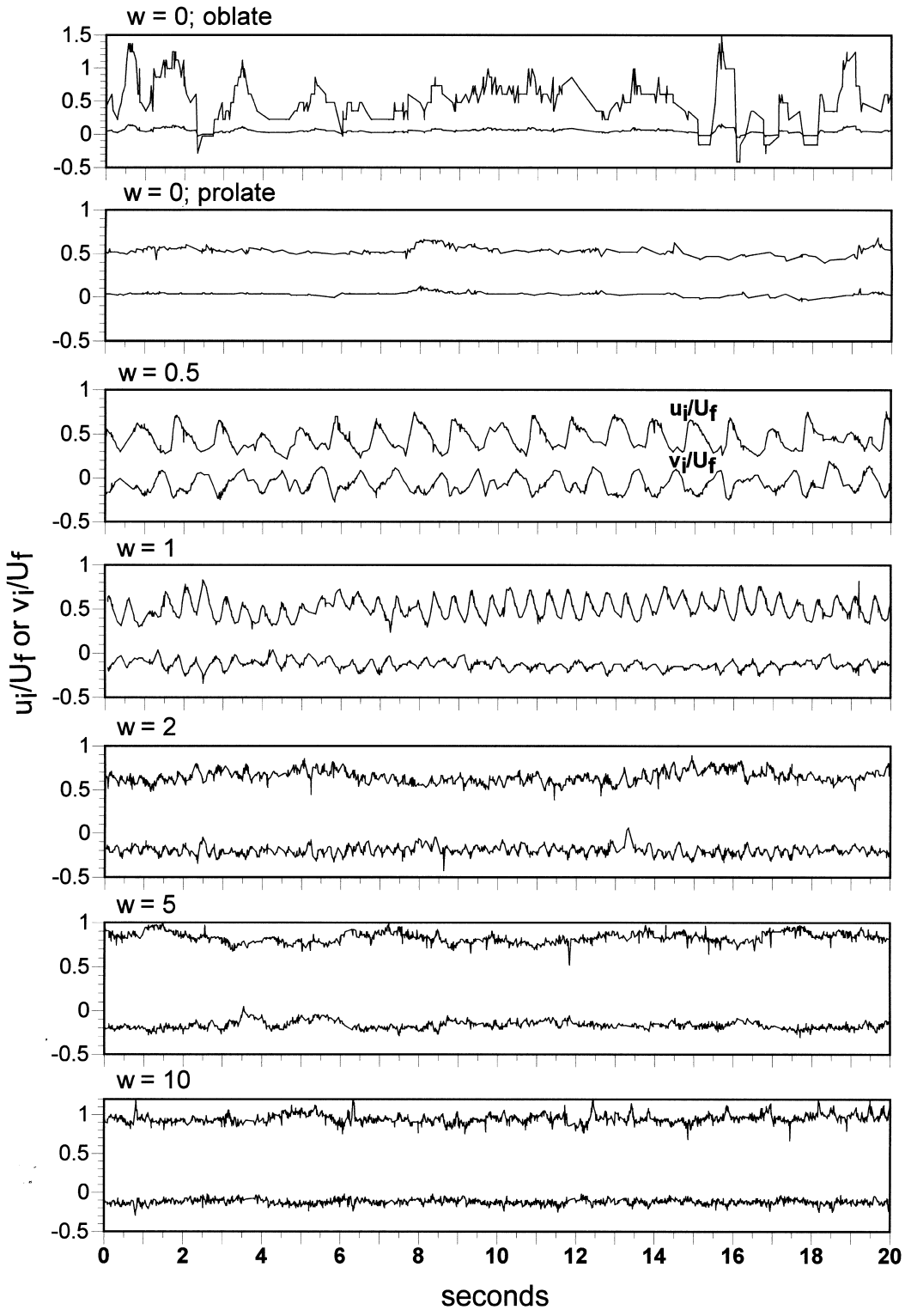

Fig. 10. Examples of time series of downstream (upper line) and vertical (lower line) components of velocity downstream of spheroid at $x/D = 2$ and $y/D = 0$ for $w = 0$, 0.5, 1, 2, 5 and 10.

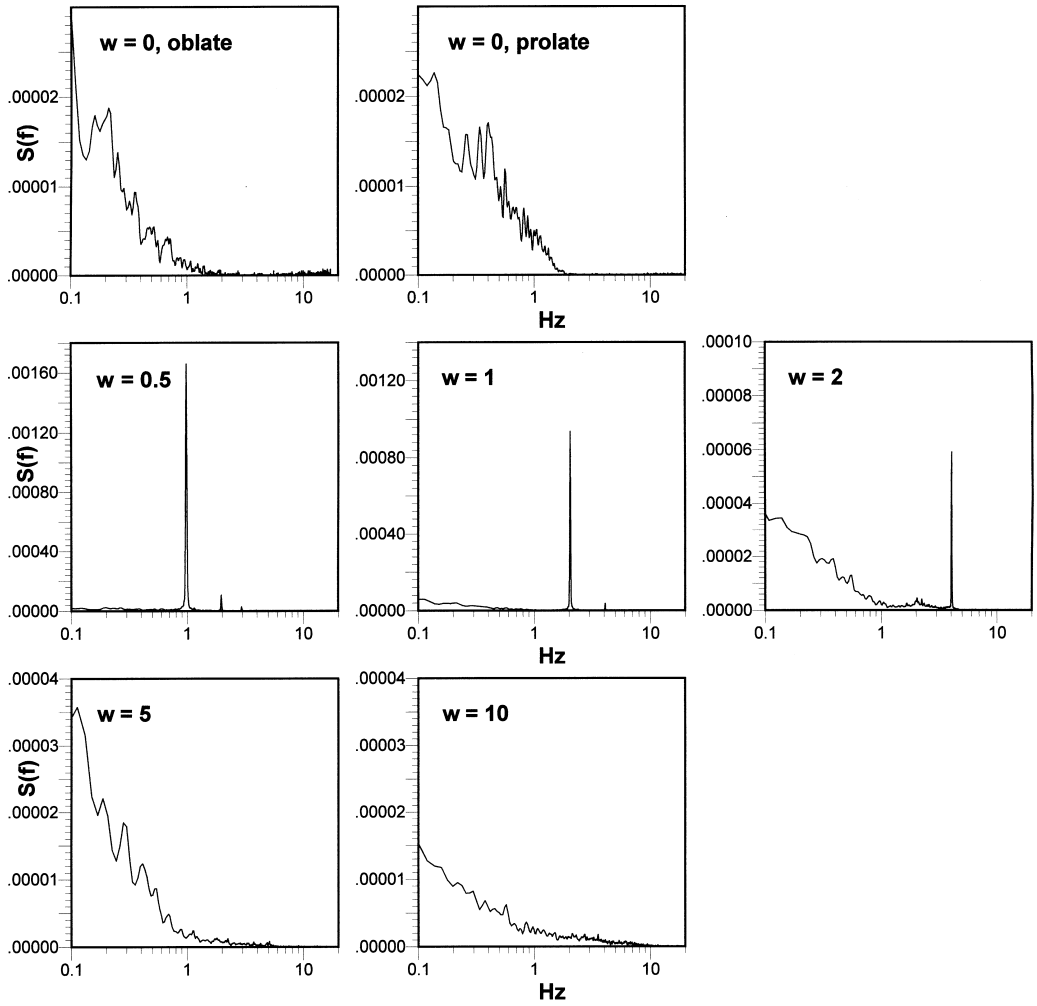

Fig. 11. Frequency spectra (spectral density, $S(f)$) derived from 600 s time series at $U_f = 0.105$, $w = 0$, 0.5, 1, 2, 5 and 10, $x/D = 2$ and $y/D = 0$ for the spheroidal particle.

the velocity structure at $w = 0.5$, 1 and 2. However, at $w = 5$ and 10 ($\beta \sim 1.5$ and 3), this modulation is absent and the time series is not dominated by a regular periodicity. Spectra of these time series (Fig. 11) beautifully capture the modulation at lower values of w. Turbulence is dominated by frequencies generally less than 1 Hz for $w = 0$ in both the oblate and prolate positions. However, at $w = 0.5$, 1 and 2 the signal is completely dominated by frequencies at twice the rate of rotation, this being caused by shedding of the wake region generated when the spheroid is in an oblate position but shed into the flow when the spheroid approaches the prolate orientation. At $w = 5$ ($\beta \sim 1.5$) this modulation has disappeared and the signal becomes dominated by both a broad spread of lower frequencies, as well as an increasing proportion of frequencies greater than 2 Hz (see also spectra for $w = 10$). It therefore appears that the trends identified around the sphere with increasing rotation rate are even more

apparent for a spheroid but are modified in frequency due to the shape of the particle. At low particle rotation rates, at approximately $\beta < 0.5$, the turbulence field downstream of the particle is dominated by wake vortices shed at twice the rotation rate. However, at higher rotation rates ($\beta > \sim 0.5$), where the wake region is destroyed or does not have time to form, this modulation disappears and, although the turbulence intensities on the lower side of the particle increase, this turbulence is not dominated by wake shedding from the particle but by shear layer instability on the lower side of the particle.

5. Discussion: particle rotation and mechanisms of turbulence enhancement in two-phase flows

These simple experiments on rotating isolated spherical and spheroidal grains at $Re_p < 300$ demonstrate how turbulence is greatly modulated by particle rotation. This process occurs through two mechanisms. For both particle shapes, at low rotation rates, where $\beta < 0.5$, the wake region both decreases in size with increasing rotation rate and becomes unstable, shedding vortices at a frequency proportional to the rotation rate. For spherical grains this rate is w, whilst for the spheroidal grain this shedding frequency is $2w$. As β exceeds 0.5, the wake region disappears and flow around the particle is dominated by generation of a strong shear layer on the underside of the grain. This shear layer is caused as flow is dragged over the top of the grain and sheared against the downstream flow on the underside of the grain; as rotation rate increases, the velocity and volume of flow entrained around the particle increases, and flow may move strongly upstream close to the underside of the grain, thereby generating an intense layer of shear in that region. Similar patterns of flow and modification to the turbulence structure have also been demonstrated experimentally for spinning circular cylinders by Díaz et al. (1983) who reasoned that the Kármán vortex activity associated with the wake was present up to peripheral cylinder velocities equivalent to the freestream velocity, but above this value the activity decreases and ceases to exist for rotation rates twice that of the freestream velocity.

It is clear that particle rotation, especially for aspherical grains, will thus have a great impact on the modulation of turbulence. When particle rotation is present, turbulence enhancement in the fluid phase may occur at particle Reynolds numbers far lower than 400 normally associated with wake instability (Achenbach 1974). Additionally, the mechanism of turbulence enhancement when $\beta > 0.5$ does not lie in wake instability but in generation of a shear layer on the underside of the grain. This highlights the fact that some current assumptions concerning the mechanisms of turbulence modulation in two-phase flow models (Yuan and Michaleides 1992; Bolio and Sinclair 1995) require revision.

In order to assess whether the rates of particle rotation required to destroy the wake region are likely to be present in a range of two-phase flows, Table 3 presents a summary of relative velocities and particle Reynolds numbers measured in past two-phase flow work using coarse sediment. These values allow an estimation of the particle rotation rates that would be required in order to destroy any wake present behind the grain (namely, where $U_p/U_{rel} > 0.5$). Firstly, it is evident that the particle Reynolds numbers calculated from estimates of the relative velocity between the two phases are generally far less than the value of 400 normally associated with wake instability (Achenbach 1974). Bolio and Sinclair (1995) also noted this fact and ascribed

Table 3
Summary of relative velocities and particle Reynolds numbers in past studies and an estimate of the particle rotation rate, w, when $U_p/U_{rel} = 0.5$ and where the wake region ceases to exist

Author(s)	Fluid	Grain type	Mean grain size μm	U_{rel} m s^{-1}	Re_p	Rotation rate, w when U_p/U_{rel}= 0.50 rps
Chandok and Pei (1972)	Air	Glass	475	3.80–5.23	105–144	1423–1959
Levy and Lockwood (1981)	Air	Sand	1060	1.44	85	216
Lee & Durst (1982)	Air	Glass	800	1.74–4.22	77–188	346–840
Tsuji and Morikawa (1982)	Air	Plastic Pellets	3430	2	378	93
Rashidi et al. (1990)	Water	Polystyrene	1100	0.0614	81	18
			650	0.0361	28	18
			220	0.0228	6	33
Kaftori et al. (1995b)	Water	Polystyrene	900	0.113–0.164	12.6–18.22	20-29
Best et al. (1997)	Water	Glass Beads	220	0.019	43	14
			275 (max^m)	0.0436	14	25

any turbulence modulation to the 'wake effect' rather than wake eddy shedding. Secondly, however, it can be seen that the rotation rates required to destroy the presence of the wake region are well within the ranges of values that have been measured in past studies, for both air and water flows (Table 1). This again confirms the contention that particle rotation may be a critical factor in controlling the production of turbulence around sediment grains in two-phase flows and calls for more detailed studies of the rates and nature of particle rotation.

Besides the significant implications of particle rotation for the mechanisms of turbulence modulation in two-phase flows, it is also apparent that the flow around rotating grains, and associated high turbulence intensities and Reynolds stresses, may provide an important contribution to the entrainment and suspension/re-suspension of very fine grained sediment. Rice et al. (1996) discuss the possible role of the wake region associated with grains in entraining finer particles during grain saltation. Although this effect will not be operative when $U_p/U_{rel} > 0.5$, the high Reynolds stresses generated around rotating grains, especially where those grains are present in high enough concentrations to undergo mutual particle interference, may serve to provide the turbulence anisotropy and velocity gradients required for suspension. It is also worthy of note that the simple experiments described in the present paper concern rotation solely in the sense of the flow shear gradient. However, grain collisions both in suspension and with the bed may (i) produce particle spin in the reverse sense to the mean shear, and, (ii) give rise to grains which move faster than the fluid, thereby generating wake regions on the *upstream* side of the grain, which may then be destabilised by rotation. Since appreciable spin rates are most likely due to grain collisions rather than the mean velocity gradient across a particle, and the likelihood that particle collisions may occur far more frequently than has been assumed until very recently (Sørensen and McEwan 1996), it appears that the role of particle rotation and its influence on both the flow field and entrainment of other grains warrants far greater study.

6. Summary

This study has examined the influence of particle rotation, for both spherical and spheroidal grains, at a range of particle Reynolds numbers less than 300. Particle rotation in the direction of the mean shear has been investigated experimentally at rotation rates from 0.5–10 rps. These rates lie well within estimates of grain rotation measured in past studies where rotation has been largely generated by particle collisions as well as by the mean fluid shear. Several principal conclusions can be drawn:

1. Grain rotation significantly influences the pattern of flow around the particle at particle Reynolds numbers less than 300 and may be a dominant mechanism of turbulence modulation associated with large grains.
2. When the ratio of the peripheral velocity of the grain to the mean relative velocity (U_p/U_{rel}) exceeds 0.5, the wake region associated with the grain is destroyed. Additionally, the length, and hence volume of the wake region are significantly modified when $0 < U_p/U_{rel} < 0.5$ as compared to measurements obtained at zero rotation. This suggests previous models of two-phase flow turbulence modulation which ignore the influence of rotation may be both

invoking the incorrect mechanisms of turbulence modulation and using overestimates of wake size.

3. Where $0 < U_p/U_{rel} < 0.5$, the frequency of vortex generation behind the particle is modulated by rotation. For spherical particles the frequency of vortex shedding is equal to w, whereas for spheroidal particles this frequency is equal to $2w$ as the particle occupies two oblate orientations in each rotation. When $U_p/U_{rel} > 0.5$ and the wake region is absent, turbulence generation is dominated by a shear layer generated on the underside of the grain, where fluid entrained by rotation and dragged around the sphere shears against the freestream flow beneath the grain. In this case, turbulence enhancement in the fluid phase may be envisaged *without* the presence of a wake region, contrary to that proposed in many past studies.
4. Comparisons with past work and estimates of relative velocities show that the range of particle rotation rates required to either significantly modify or destroy the wake region are well within measured rotation rates in both air and water flows.
5. Significant particle rotation, especially near the wall where grain-wall collisions are important and higher sediment concentrations are present, is likely to be the norm rather than the exception in most two-phase flows. The influence of rotation must therefore be included in both mechanistic interpretations of turbulence modulation and more complete numerical models of sediment-fluid coupling.

Acknowledgements

I would like to acknowledge the support of the UK Natural Environment Research Council (Grant GR3/8235) and the Nuffield Foundation for a Science Research Fellowship which allowed this work to be developed and implemented. I am also indebted to Neil Woodhouse for his technical assistance in running the experiments, Stuart McLelland for valuable discussions and Phil Fields, Tony Windross and Bob Bowes for their construction of the oil flume and particle rotation rig. Derek Ingham, Lionel Elliott, Henry Pantin and two referees are thanked for their thorough and constructive comments on this paper.

References

Achenbach, E., 1974. Vortex shedding from spheres. J. Fluid Mechanics 62, 209–221.

Badr, H.M., Dennis, S.C.R., Ingham, D.B., 1989. Steady and unsteady flow past a rotating circular cylinder at low Reynolds numbers. Computers and Fluids 17, 579–609.

Barkla, H.M., Auchterlonie, L.J., 1971. The Magnus or Robins effects on rotating spheres. J. Fluid Mechanics 47, 437–447.

Best, J., Bennett, S., Bridge, J., Leeder, M., 1997. Turbulence modulation and particle velocities over flat sand beds at low transport rates. J. Hydraulic Engineering 123, 1118–1129.

Bolio, E.J., Sinclair, J.L., 1995. Gas turbulence modulation in the pneumatic conveying of massive particles in vertical tubes. Int. J. Multiphase Flow 21, 985–1001.

Chandok, S.S., Pei, D.C.T., 1972. Particle dynamics in solids–gas flow in a vertical pipe. In: Hetsroni, G., Sideman, S., and Hartnett, J.P. (Eds.), Progress in Heat and Mass Transfer, 6, pp. 465–474.

Chepil, W.S., 1945. Dynamics of wind erosion. I. Nature of soil movement by wind. Soil Sci. 60, 305–320.

Clift, R., Grace, J.R, Weber, M.E., 1978. Bubbles, Drops and Particles, Academic Press, New York, p. 380.

Crowe, C.T., 1993. Modelling turbulence in multiphase flows. In: Rodi, W., Martelli, F. (Eds.), Engineering Turbulence Modelling and Experiments 2, Elsevier, Amsterdam, pp. 899–913.
Crowe, C.T., Troutt, T.R., Chung, J.N., 1996. Numerical models for two-phase turbulent flows. Ann. Review of Fluid Mechanics 28, 11–43.
DANTEC, 1994. PDA Installation and Users Guide. DANTEK Electronik.
Díaz, F., Gavaldà, J., Kawall, J.G., Keffer, J.F., Giralt, F., 1983. Vortex shedding from a spinning cylinder. Physics of Fluids 26, 3454–3460.
Elghobashi, S., 1994. On predicting particle-laden turbulent flows. Applied Scientific Research 52, 309–329.
Elghobashi, S., Truesdell, G.C., 1993. On the two-way interaction between homogeneous turbulence and dispersed solid particles. I: Turbulence modification. Physics of Fluids A 5, 1790–1801.
Francis, J.R.D., 1973. Experiments on the motion of solitary grains along the bed of a water-stream. Proc. Royal Soc. Lond. A 332, 443–471.
Gore, R.A., Crowe, C.T., 1989a. Effect of particle size on modulating turbulent intensity. Int. J. Multiphase Flow 15, 279–285.
Gore, R.A., Crowe, C.T. 1989b. Effect of particle size on modulating turbulent intensity: influence of radial location. In: Michaelides, E.E., Stock, D.E. (Eds.), Turbulence Modification in Dispersed Multiphase Flows, 80, ASME FED, pp. 31–35.
Gore, R.A., Crowe, C.T., 1991. Modulation of turbulence by a dispersed phase. Trans. Am. Soc. Mech. Engnrs, J. Fluids Engrg. 113, 304–307.
Hardalupas, Y., Taylor, A.M.K.P., Whitelaw, J.H., 1989. Velocity and particle-flux characteristics of turbulent particle-laden jets. Proc. Royal Soc. London A 426, 31–78.
Hardalupas, Y., Taylor, A.M.K.P., Whitelaw, J.H., 1992. Particle dispersion in a vertical round sudden-expansion flow. Proc. Royal Soc. London A 341, 411–442.
Hetsroni, G., 1989. Particles–turbulence interaction. Int. J. Multiphase Flow 5, 735–746.
Hetsroni, G. 1993. The effect of particles on the turbulence in a boundary layer. In: Roco, M.C. (Ed.), Particulate Two-phase Flow., Butterworth-Heinemann, pp. 244–264.
Hui, Y., Hu, E., 1991. Saltation characteristics of particle motions in water. Shuili Xuebao 12, 59–64 (in Chinese).
Ingham, D.B., 1983. Steady flow past a rotating cylinder. Computers & Fluids 4, 351–366.
Ingham, D.B., Tang, T., 1990. A numerical investigation into the steady flow past a rotating circular cylinder at low and intermediate Reynolds numbers. J. Computational Physics 87, 91–107.
Kaftori, D., Hetsroni, G., Banerjee, S., 1995a. Particle behaviour in the turbulent boundary layer. I. Motion, deposition and entrainment. Physics of Fluids 7, 1095–1106.
Kaftori, D., Hetsroni, G., Banerjee, S., 1995b. Particle behaviour in the turbulent boundary layer. II. Velocity and distribution profiles. Physics of Fluids 7, 1107–1121.
Kalra, T.R., Uhlherr, P.H.T., 1973. Geometry of bluff body wakes. Canadian J. Chemical Engineering 51, 655–658.
Kenning, V.M., Crowe, C.T., 1997. On the effect of particles on carrier phase turbulence in gas–particle flows. Int. J. Multiphase Flow 23, 403–408.
Kulick, J.D., Fessler, J.R., Eaton, J.K., 1993. On the interactions between particles and turbulence in a fully-developed channel flow in air. Report MD-66, Thermosciences Division, Dept. of Mechanical Engrg.. Stanford Univ., California.
Kulick, J.D., Fessler, J.R., Eaton, J.K., 1994. Particle response and turbulence modification in fully developed channel flow. J. Fluid Mechanics 277, 109–134.
Lee, H.-Y., Hsu, I.-S., 1994. Investigation of saltating particle motions. J. Hydraulic Engineering 120, 831–845.
Lee, H.-Y., Hsu, I.-S., 1996. Particle spinning motion during saltation process. J. Hydraulic Engineering 122, 587–590.
Lee, S.L., Durst, F., 1982. On the motion of particles in turbulent duct flows. Int. J. Multiphase Flow 8, 125–146.
Levy, Y., Lockwood, F.C., 1981. Velocity measurements in a particle laden turbulent free jet. Combustion and Flame 40, 333–339.
Liang, S.-C., Hong, T., Fan, L.-S., 1996. Effects of particle arrangements on the drag force of a particle in the intermediate flow regime. Int. J. Multiphase Flow 22, 285–306.
Masliyah, J.H., 1972. Steady wakes behind oblate spheroids: flow visualisation. Physics of Fluids 15, 1144–1146.
Masliyah, J.H., Epstein, N., 1970. Numerical study of steady flow past spheroids. J. Fluid Mechanics 44, 493–512.
Nalpanis, P., Hunt, J.C.R., Barrett, C.F., 1993. Saltating particles over flat beds. J. Fluid Mechanics 251, 661–685.
Nezu, I., Nakagawa, H., 1993. Turbulence in open-channel flows. Int. Ass. Hydraul. Res. Monograph Series. A. A. Balkema, Rotterdam.
Niño, Y., García, M., 1994. Gravel saltation: modeling. Water Resources Research 30, 1915–1924.
Poe, G.G., Acrivos, A., 1975. Closed-streamline flows past rotating single cylinders and spheres: inertia effects. J. Fluid Mechanics 72, 605–623.
Rashidi, M., Hetsroni, G., Banerjee, S., 1990. Particle-turbulence interaction in a boundary layer. Int. J. Multiphase Flow 16, 935–949.
Rayan, M.A., 1980. Influence of solid particles in suspension on some turbulent characteristics. In: Multiphase Transport: Fundamentals, Reactor Safety, Applications, Volume 4. Hemisphere Publ. Co., New York, pp. 1969–1991.

Rice, M.A., Willetts, B.B., McEwan, I.K., 1996. Observations of collisions of saltating grains with a granular bed from high-speed cine-film. Sedimentology 43, 21–32.
Rimon, Y., Cheng, S.I., 1969. Numerical solution of a uniform flow over a sphere at intermediate Reynolds numbers. Physics of Fluids 12, 949–959.
Rogers, C.B., Eaton, J.K., 1990. The behaviour of solid particles in a vertical turbulent boundary layer in air. Int. J. Multiphase Flow 16, 819–834.
Rogers, C.B., Eaton, J.K., 1991. The effect of small particles on fluid turbulence in a flat-plate, turbulent boundary layer in air. Physics of Fluids A 3, 928–937.
Rubinow, S., Keller, J., 1961. The transverse force on a spinning sphere moving in a viscous fluid. J. Fluid Mechanics 11, 447–459.
Saffman, P.G., 1965. The lift on a small sphere in a slow shear flow. J. Fluid Mechanics 22, 385–400.
Shuen, J-S., Solomon, A.S.P., Zhang, Q-F., Faeth, G.M., 1985. Structure of particle-laden jets: measurements and predictions. J. Amer. Inst. Aeronautics and Astronautics 23, 396–404.
Sørensen, M., McEwan, I., 1996. On the effect of mid-air collisions on aeolian saltation. Sedimentology 43, 65–76.
Taneda, S., 1956. Experimental investigation of the wake behind a sphere at low Reynolds numbers. J. Physical Soc. Japan 11, 1104–1108.
Taneda, S., 1978. Visual observations of the flow past a circular cylinder performing a rotatory oscillation. J. Physical Soc. Japan 45, 1038–1043.
Townsend, P., 1980. A numerical simulation of Newtonian and visco-elastic flow past stationary and rotating cylinders. J. Non-Newtonian Fluid Dynamics 6, 219–243.
Tsuji, Y., Morikawa, Y., 1982. LDV measurements of an air-solid two-phase flow in a horizontal pipe. J. Fluid Mechanics 120, 385–409.
Tsuji, Y., Morikawa, Y., Shiomi, H., 1984. LDV measurements of an air-solid two-phase flow in a vertical pipe. J. Fluid Mechanics 139, 417–434.
Tsuji, Y., Morikawa, Y., Mizuno, O., 1985. Experimental measurement of the Magnus force on a rotating sphere at low Reynolds numbers. Transactions of the American Society of Mechanical Engineers 107, 484–488.
Tsuji, Y., Morikawa, Y., Terashima, K., 1982. Fluid-dynamics interaction between two spheres. Int. J. Multiphase Flow 8, 71–82.
White, B.R., 1982. Two-phase measurements of saltating turbulent boundary layer flow. Int. J. Multiphase Flow 8, 459–473.
White, B.R., 1986 Particle transport by atmospheric winds on Venus: an experimental wind tunnel study. In: Nickling, W.G. (Ed.), Aeolian Geomorphology, Allen and Unwin, London, pp. 57–73.
White, B.R., Schulz, J.C., 1977. Magnus effect in saltation. J. Fluid Mechanics 81, 497–512.
Willetts, B.B., 1983. Transport by wind of granular materials of different grain shapes and densities. Sedimentology 30, 669–679.
Willetts, B.B., Rice, M.A., 1986. Collisions in aeolian transport. Acta Mechanica 63, 255–265.
Willetts, B.B., Rice, M.A., Swaine, S.E., 1982. Shape effects in aeolian grain transport. Sedimentology 29, 409–417.
Yarin, L.P., Hetsroni, G., 1994a. Turbulence intensity in dilute two-phase flows - 1. Effect of particle-size distribution on the turbulence of the carrier fluid. Int. J. Multiphase Flow 20, 1–16.
Yarin, L.P., Hetsroni, G., 1994b. Turbulence intensity in dilute two-phase flows - 3. The particles-turbulence interaction in dilute two-phase flow. Int. J. Multiphase Flow 20, 27–44.
Yuan, Z., Michaelides, E.E., 1992. Turbulence modulation in particulate flows — a theoretical approach. Int. Journal Multiphase Flow 18, 779–785.
Zhu, C., Liang, S.-C., Fan, L.-S., 1994. Particle wake effects on the drag force of an interactive particle. Int. J. Multiphase Flow 21, 117–129.